Ultramicroscopy 111 (2011) 1338–1342

Contents lists available at ScienceDirect

Ultramicroscopy

journal homepage: www.elsevier.com/locate/ultramic

# Ion beam nanopatterning and micro-Raman spectroscopy analysis on HOPG for testing FIB performances

B.S. Archanjo [a,*], I.O. Maciel [c], E.H. Martins Ferreira [a], S.B. Peripolli [a], J.C. Damasceno [a], C.A. Achete [a,b], A. Jorio [a,c]

[a] Divisão de Metrologia de Materiais, Instituto Nacional de Metrologia, Normalização e Qualidade Industrial (INMETRO), Duque de Caxias 25250-020, Rio de Janeiro, RJ, Brazil
[b] Programa de Engenharia Metalúrgica e de Materiais (PEMM), Universidade Federal do Rio de Janeiro, Cx. Postal 68505, CEP 21945-970, Rio de Janeiro, RJ, Brazil
[c] Departamento de Física, Universidade Federal de Minas Gerais, MG 30123-970, Belo Horizonte, Minas Gerais, Brazil

ARTICLE INFO

*Article history:*
Received 29 July 2010
Received in revised form
6 April 2011
Accepted 24 April 2011
Available online 29 April 2011

*Keywords:*
Focused ion beam
HOPG
Raman spectroscopy
Metrology

ABSTRACT

This work reports $Ga^+$ focused ion beam nanopatterning to create amorphous defects with periodic square arrays in highly oriented pyrolytic graphite and the use of Raman spectroscopy as a new protocol to test and compare progresses in ion beam optics, for low fluence bombardment or fast writing speed. This can be ultimately used as a metrological tool for comparing different FIB machines and can contribute to Focused Ion Beam (FIB) development in general for tailoring nanostructures with higher precision. In order to do that, the amount of ion at each spot was varied from about $10^6$ down to roughly 1 ion per dot. These defects were also analyzed by using high resolution scanning electron microscopy and atomic force microscopy. The sensitivities of these techniques were compared and a geometrical model is proposed for micro-Raman spectroscopy in which the intensity of the defect induced *D* band, for a fixed ion dose, is associated with the diameter of the ion beam. In addition, the lateral increase in the bombarded spot due to the cascade effect of the ions on graphite surface was extracted from this model. A semi-quantitative analysis of the distribution of ions at low doses per dot or high writing speed for soft modification of materials is discussed.



## 1. Introduction

Focused ion beam (FIB) technology is a powerful technique to change material properties at nano- and microscale. A FIB microscope has a well controlled spot positioning with a beam diameter of nanometer range. These features allow controlled deposition and removal of materials, ion implantation and amorphization on the surface of many desirable substrates. Therefore this technique improves our knowledge about physical systems at nano- or microscale range, and also about the use of nanopatterning and nanostructuring to fabricate nanodevices [1,2].

Since seminal studies in the beginning of 1980s, much effort has been done to improve and test the ultimate capabilities of FIB technique [1,2]. In this direction, some works have been published by J. Gierak and collaborators developing and testing the ultimate resolutions of FIB microscopes in many different materials. In special, there is a recently published review [3] and few studies using FIB technology as a tool to modify highly oriented pyrolytic graphite (HOPG) surface in order to employ it as template for self-assembling of particles and molecules [4–6]. Also, several methods were applied to understand the $Ga^+$ ion-HOPG interaction, including atomic force microscopy (AFM), micro-Raman spectroscopy (RS) and computer simulation [3–11].

Raman spectroscopy is a well established technique to study the disorder in crystalline systems, especially in carbon materials such as graphite, carbon nanotubes and graphene [12–21]. The Raman spectrum between 1000 and 2000 $cm^{-1}$ of defect-free HOPG exhibits a single sharp peak around 1580 $cm^{-1}$, named *G* peak, which is related to the in-plane stretching of the C–C bonds in the graphene sheet. When defects are present, two additional peaks, named *D* and *D′* are observed at ~1360 and ~1620 $cm^{-1}$, respectively; the *D′* peak being normally much weaker than the *D* and *G* peaks [12]. The relative intensity of the *D* and *G* peaks, $I_D/I_G$, is routinely used as a measure of the degree of disorder in carbon materials. For instance, in disordered graphite $I_D/I_G$ is inversely proportional to the microcrystallite size [17–20]. In such materials, the *D* peak intensity increases with the density of defects until the graphite becomes amorphous and the Raman spectrum turns into a broad band [12–21].

This work reports further improvements to understand the $Ga^+$ ion implantation on HOPG using a FIB source at small level of modification. The sensitivity on probing defects on HOPG surface is investigated by using scanning electron microscopy (SEM), atomic force microscopy (AFM) and micro-Raman Spectroscopy (RS).

* Corresponding author. Tel.: +552126799798; fax: +552126799021.
*E-mail address:* bsarchanjo@inmetro.gov.br (B.S. Archanjo).

0304-3991/$ - see front matter © 2011 Elsevier B.V. All rights reserved.
doi:10.1016/j.ultramic.2011.04.007

RS showed the highest sensitivity among the techniques used in this study and it was capable of resolving spatial distribution of ion implantation at low fluences and high writing speed. The lateral cascade effect caused by ion implantation on HOPG is indirectly measured using a simple phenomenological model. Also a method to estimate the beam blank and writing speed performance is proposed and discussed. Therefore, in the metrological point of view, the bombardment of HOPG and RS is used as a new approach to test and compare progresses in ion beam optics for soft and precise modifications, which can be achieved in low fluence bombardment and accurate spot positioning.

## 2. Material and methods

The sample used is a HOPG purchased from NT-MDT company (HOPG ZYB grade, $20 \times 20 \times 2$ mm). Before ion bombardment the sample is cleaved using a common adhesive tape. AFM analysis was carried out with a Nano Wizard AFM (JPK) operated in intermittent contact mode, where topographic and lock-in phase images are recorded simultaneously. The bombardments and FEG-SEM high resolution images were performed using a Nova Nanolab 600 dual beam platform from FEI. The patterns were performed by using a patterning tool software where the beam is opened during each pattern pass and is blanked in the end of it. The SEM images are acquired in the same equipment using a 10 keV accelerating energy and 0.13 nA electron current. The ion bombardments are executed using a $Ga^+$ ion source working at 30 keV accelerating energy with an ion current of about 1.6 pA and different dwell times (writing speeds) of 4.6 ms down to 100 ns per dot. According to the Dual Beam manufacturer, the smaller FWHM beam diameter using this current is about 7 nm. RS measurements were performed using a Horiba Jobin–Yvon T64000 triple-monochromator spectrometer in the backscattering configuration, equipped with $N_2$ cooled CCD detector and a microscope with a $100\times$ objective. The excitation laser energy was 2.41 eV (514.5 nm).

## 3. Results and discussions

### 3.1. Sensitivity of the probing techniques

The experiment started using a high ion per dot (ipd) dose of about $10^6$ ipd with spots distributed in a square lattice and spaced by 200 nm (unit cell area of $200 \times 200$ nm$^2$ with one bombarded spot). The result was observed via SEM and topographic AFM images and it is shown in Figs. 1a and b. Although the result of such a large fluence bombardment can be seen in a FEG-SEM image working in a high resolution mode, it presents a low contrast. The image in Fig. 1a shows a contrast limit of FEG to analyze HOPG bombardment is at large fluence. However, the pattern can be easily observed in AFM topographic image (Fig. 1b). As pointed out in literature [11], AFM topographic images show the volcano-like structure and its origin is related to stress and plastic relaxations and also to redeposition of materials removed from the center of the bombarded region.

The observation of the patterned region using a FEG-SEM equipment is compromised when smaller doses are used or when the distance between dots is reduced. But it is easy to observe the patterns in these conditions using an AFM apparatus, as shown in Fig. 2. Figs. 2a and b, respectively, show the topographic and lock-in phase images of a region where $2.5 \times 10^3$ ipd were used in square lattice with a unit cell of $100 \times 100$ nm$^2$. Figs. 2c and d similarly show the AFM topographic and phase images of a patterned region with $1.0 \times 10^3$ ipd in the same dot array. Although the topographic height of the spots is very low at these patterns ($< 1$ nm), the lock-in phase images show enough contrast, which is related to changes in mechanical properties of the surface at the center of the bombarded region. Furthermore, in this low fluence dose, the effect of bombardment is simply a local amorphization of the HOPG surface [11], with no removal and redeposition of material, making the size of the bombarded spots smaller than those shown in Fig. 1. Direct measurements of the overall diameter of the bombarded spot give values around 30 nm, which are in agreement with those values previously obtained via Monte Carlo simulation of 7–8 nm FWHM ion beam diameter in HOPG [4,10].

For some applications where softer amorphization or ion implantation are needed, low ion doses ($< 10^3$ ipd) are required. Examples of possible applications of such low fluence bombardment can be seen in earlier studies [21–24], where conductive properties are changed in graphite foils (graphene) by extrinsic disorder such as vacancies, adatoms and extended defects (cracks and edges). Therefore, a possible approach to produce such samples is to use a high resolution FIB with very accurate spot positioning ($\sim$2 nm), beam blank and high writing speed (dwell time of hundreds of nanoseconds).The fastest dwell time available in the FIB technology used in this study is about 100 ns, which means that the dose is in average 1 ipd. In new developed equipments, the manufacturers assure even a higher writing speed (dwell time of about 25 ns), which means a more precise

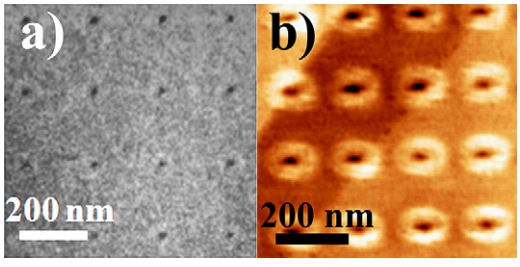


**Fig. 1.** Images of single extended defects at large fluence ion bombardment of $10^6$ ipd distributed in a square network pattern of $200 \times 200$ nm$^2$ unit cell: (a) FEG-SEM high resolution image, collected at 10 keV accelerating voltage; (b) intermittent contact AFM topographic image of the same region shown in b using a $z$ scale of 7 nm.

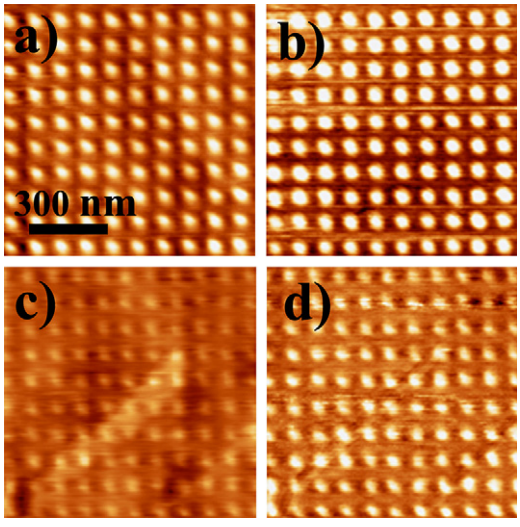


**Fig. 2.** Intermittent contact AFM images of single extended defects at low fluence distributed in a square network pattern of $100 \times 100$ nm$^2$ unit cell: (a) topographic ($z$ scale 2 nm) and (b) phase image ($z$ scale 17°) of $2.5 \times 10^3$ ipd bombardment; (c) topographic ($z$ scale 2 nm); (d) phase image ($z$ scale 17°) of a lower fluency $1.0 \times 10^3$ ipd bombardment.

distribution of bombarded patterns in low amount of ions per pixel. Although the electronics of these FIB equipments provide dwell times of 100 ns or smaller, the ion optics is not able to address the ions accurately in such fast writing speeds. In other words 1 ipd patterning scheme for arrays of dots is surely not realistic when one consider the source emission limitations used in FIB machines. An easy test can be done by using a silicon substrate and SEM image to examine the quality of the generated patterns and settle the limit of the writing speed to get trustable small ipd amounts [25].

As discussed above, soft modification is important for studies at nano and micro scales, but neither a high resolution FEG-SEM, working in the condition pointed here, nor an atomic force microscope can probe the produced defects. For fluences lower than $10^3$ ipd and small distances between the spots ( $<30$ nm), RS is used to characterize the samples, which shows that this technique is highly sensitive to the presence of defects in HOPG surface. This is easily seen in Fig. 3 which shows the evolution of the Raman spectrum with decreasing ion doses from $10^2$ down to 2 ipd in a pattern where the spots are spaced in a square network by 10 nm. Fig. 3 illustrates that, for higher ion per dot amounts, both *G* and *D* peaks turn into broader lines revealing that the HOPG surface becomes more amorphous, as expected.

This experiment demonstrates that RS is sensitive enough to probe different small ion per dot doses even when the distance between the dots is very small. Additionally, this technique can be used to study how the ions are distributed on the surface in HOPG. This can be done by labeling the density of ions implanted on the surface of HOPG in units of ions/cm$^2$. In Fig. 4 there are two plots showing the Raman spectra for two different ions/cm$^2$ doses, namely, $2.5\times10^{13}$ ions/cm$^2$ (Fig. 4a) and $1.0\times10^{13}$ ions/cm$^2$ (Fig. 4b). The difference between the two curves in each plot is how the ions are distributed on the HOPG surface. In Fig. 4a, the ions are distributed in a square network ($\sim$20 nm spot distances) with $1.0\times10^2$ ipd (red curve) and in a $100\times100$ nm$^2$ unit cell with $2.5\times10^3$ ipd (black curve). In Fig. 4b the red plot consists of ions distributed in a square lattice of $10\times10$ nm$^2$ unit cell with $1.0\times10^1$ ipd, whereas the black plot has $1.0\times10^3$ ipd in a $100\times100$ nm$^2$ unit cell of a square pattern.

In both the experiments, for the same dose per area (ions/cm$^2$) Raman spectra tell us that the more dispersed the ions on the HOPG surface (smaller the distances between the dots), the more intense the $I_D/I_G$ ratio, which means a larger defective surface area. These differences in the $I_D/I_G$ ratio for the same dose per area show us that RS is sensitive to the spot profiles in the nanometer range.

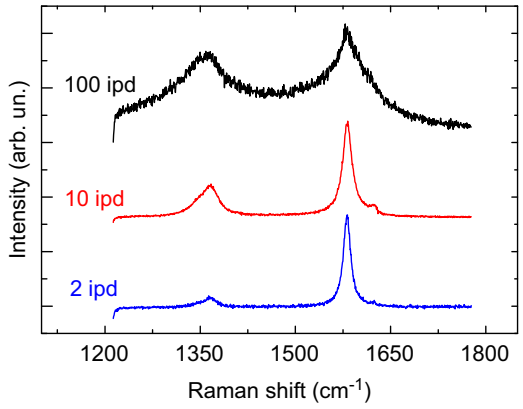


**Fig. 3.** Raman spectra of bombarded HOPG, comparing three different ion doses at the same square network pattern of $10\times10$ nm$^2$ unit cell where the doses are 100 ipd (black line), 10 ipd (red line) and 2 ipd (blue line). (For interpretation of the references to color in this figure legend, the reader is referred to the web version of this article.)

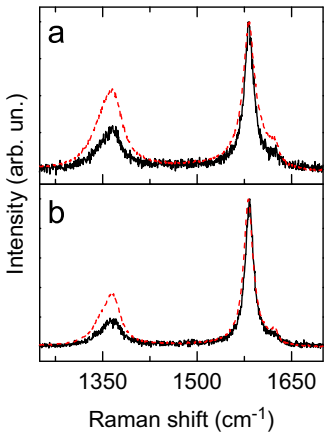


**Fig. 4.** Raman spectra of two different doses distributed on HOPG surface for different amounts of ions per dot: (a) $2.5\times10^{13}$ ion/cm$^2$ at pattern of $20\times20$ nm$^2$ unit cell with $1.0\times10^2$ ipd (red line) and $100\times100$ nm$^2$ with $2.5\times10^3$ ipd (black line); (b) $1.0\times10^{13}$ ion/cm$^2$ at $10\times10$ nm$^2$ unit cell pattern with 10 ipd (red line) and $100\times100$ nm$^2$ pattern with $1.0\times10^3$ ipd (black line). (For interpretation of the references to color in this figure legend, the reader is referred to the web version of this article.)

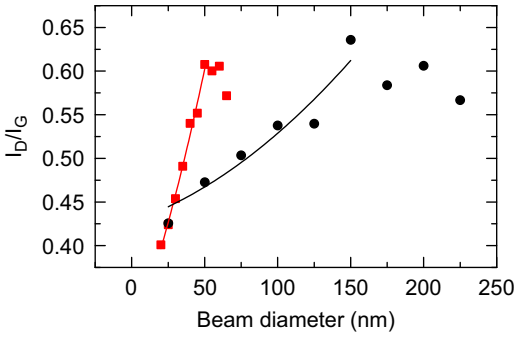


**Fig. 5.** Intensity ratio of *D* and *G* Raman peaks as functions of beam diameter for the same ion dose of $2.5\times10^{13}$ ion/cm$^2$ in two different square patterns sets, namely: $100\times100$ nm$^2$ unit cell pattern at $2.5\times10^3$ ipd (square shape red plot) and, $200\times200$ nm$^2$ unit cell pattern at $1.0\times10^4$ ipd (rounded shape black plot). Dots are experimentally collected and the continuous lines are the fitting to the experimental data. (For interpretation of the references to color in this figure legend, the reader is referred to the web version of this article.)

### 3.2. *Cascade effect of the ion beam in HOPG and dwelling time.*

Through the *D* band analysis, RS allows a measurement of the ion beam spreading at the surface of the HOPG and can be used to compare and calculate the ion beam writing fidelity to a desired pattern. However, for a given ion dose, the calibration of the *D* band intensity is needed. In order to make this possible, two bombardment sets were performed, with a constant ion dose of $2.5\times10^{13}$ ion/cm$^2$. In each subsequent bombardment set, the beam diameter (as it arrives on the HOPG surface) is increased by defocusing the beam optically. Fig. 5 shows the normalized intensity of the *D* band ($I_D/I_G$) for two different patterns as the ion beam diameter increases. The values of the beam diameter were obtained from the microscope software which completely agree with the values of the beam diameter measured directly from secondary electrons images generated by the primary ion beam (Figure S5 on Ref. [25]). Round symbols are the experimental data collected from a pattern in which the ion dose at HOPG substrate is $1.0\times10^4$ ipd in a $200\times200$ nm$^2$ unit cell square pattern. The square symbols come from a pattern where the ion dose is $2.5\times10^3$ ipd in a $100\times100$ nm$^2$ unit cell square pattern. The continuous lines are obtained by fitting the data using a geometric phenomenological model, where we suppose that the

defects are distributed on HOPG structure in a cylindrical geometry [10,25] and it is expressed by the following equation:

$$I_D/I_G = K_I - K_{II}[A_l - \pi(R_b + R_s)^2]$$

where $K_I$ is the saturation value of $I_D/I_G$ ratio when the ion dose is completely spread out, $K_{II}$ is a fitting parameter, $A_l$ is the unit cell area, $R_b$ is the beam radius and $R_s$ is the increase in the overall radius due to the multiple scattering of $Ga^+$ ions on HOPG surface (lateral cascade effect shown in Figures S3 and S4 in Ref. [25]). For the dose applied here ($2.5\times10^{13}$ ion/cm$^2$), the $K_I$ value is about 0.6. For the $100\times100$ nm$^2$ pattern (round shape symbols), the adjusting values obtained are $K_{II}=(4.4\pm0.1)\times10^{-5}$ nm$^{-2}$ and $R_s=(16\pm1)$ nm. For the $200\times200$ nm$^2$ pattern (black plot), we have $K_{II}=(5.5\pm0.1)\times10^{-6}$ nm$^{-2}$ and $R_s=(17\pm1)$ nm. Therefore, using the minimum ion beam FWHM, which according to the equipment manufacturer [25] is about 7 nm, the diameter of the bombarded spot size including beam-sample interactions on HOPG surface is about 40 nm. This value agrees with the results obtained directly from topographical images shown in Figs. 2a and c. Also, analyzing these results in both different pattern experiments, the diameter of the cascade effect is in accordance with the results obtained via Monte Carlo simulation present in literature [4,10], where the vacancy density caused by an 7–8 nm FWHM diameter ion beam on HOPG has a total diameter size of the bombarded area between 30 and 40 nm.

Comparing the constant $K_{II}$ in both experiments, one can see that for the $200\times200$ nm$^2$ pattern, this value is about ten times smaller than the value for the $100\times100$ nm$^2$ pattern. This is simply due to the fact that, in the $100\times100$ nm$^2$ pattern the non defective area that decreases with the increasing of $K_{II}$ reduces faster with respect to the beam diameter because the distance between spot is smaller. Also when the spot distance increases as in the $200\times200$ nm$^2$ pattern, a large spot had to be used to achieve the saturation of the *D* band. Therefore, the geometry of the beam-HOPG cascade effect and the creation of defects due to beam tail [3] can cause more defects in patterns where the distances between the dots are smaller. The created defects can then increase the modified area by reducing the defect-free area accordingly.

Another important parameter in ion beam patterning is the dwell time, since together with the ion beam current it controls the amount of ions arriving at each spot in a desired pattern. A study of this effect in ion patterning is relevant because, as already stated, the electronic of the ion column used in this study is able to deliver 1 ipd in average, but this low fluence is limited by the optics of the ion source (Figure S1 and S2 in support information [25]). After we correlate the $I_D/I_G$ ratio to the total beam diameter including the cascade effect, we can also use it to study the effect of writing speed in the bombarded spot profile. We created a semi-quantitative methodology to test the spatial accuracy of the ion beam distribution on a HOPG surface with the decreasing of the dwell time (writing speed) by means of micro-Raman spectroscopy. In this experiment five square patterns of $200\times200$ nm with $1.0\times10^4$ ipd are produced with different dwell times. In order to keep the ions per dot constant, the number of times that each site in the surface is bombarded was varied accordingly. The dwell time and number of bombardments per site were varied from 1 ms and 1 pass per site to 100 ns and $10^4$ passes per site. Fig. 6 shows a plot of $I_D/I_G$ as function of the dwell time. The $I_D/I_G$ ratio remains almost constant and below 0.45 until the dwell time reaches the value of 10 μs. For a dwell time below 1 μs (~10 ipd with the lowest current of 1.6 pA), the $I_D/I_G$ increases. This indicates that the pattern does not have perfect and small spots (as shown in the images S1d and S2d [25]). In fact, for a dwell time of 100 ns, the $I_D/I_G$ ratio gets very close to 0.6, which means that the overall effect of the pattern on the HOPG surface is similar to that obtained when the beam defocuses plus the cascade effect is of the order of the spot distances. Therefore for fast dwell times, which provide low fluence bombardments, the optical limitations play an important role, preventing the use of FIB systems for creating well defined patterns in these conditions.

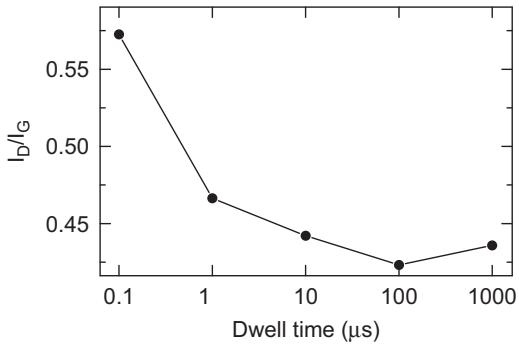


**Fig. 6.** Intensity ratio of *D* and *G* Raman peaks as function of dwell time at an ion dose of $2.5\times10^{13}$ ion/cm$^2$ in a $200\times200$ nm$^2$ unit cell pattern with $1.0\times10^4$ ipd.

## 4. Conclusion

In this work, the performance of ion beam nanopatterning was tested on the surface of HOPG and verified using FEG-SEM, AFM and micro-Raman spectroscopy (RS). The sensitivity of these techniques were tested and compared, and we found that the RS has the best sensitivity to probe the defects and it differentiates patterns with the same ion dose per area but having differences in the spot profile in the nanometer range. A simple geometrical model was proposed in order to use the intensity of the *D* band of the Raman spectrum as a measurement of the defect spatial distribution caused by the ion beam spreading out on HOPG surface. Also, the mean diameter of the cascade effect is extracted from this geometrical model. In addition, these results show that the RS measurements of bombarded HOPG can be used to test the performance of the FIB equipment and set parameters to study other materials in a fast and easy way, bringing new insights for future experiments to obtain the standard deviation of the measurements. Also, RS provides a new approach in order to understand the capabilities and damage of FIB technique for tailoring nanostructures such as nanoribbons and graphene structures for nanodevices applications with great precision and low modification level.

## Acknowledgments

The authors acknowledge the financial support from the Brazilian Agencies CNPq, FINEP and FAPERJ.

## Appendix A. Supplementary material

Supplementary data associated with this article can be found in the online version at doi:10.1016/j.ultramic.2011.04.007

## References

[1] R.L. Seliger, J.W. Ward, V. Wang, R.L. Kubena, Appl. Phys. Lett. 34 (1979) 310.
[2] L.A. Giannuzzi, Introduction to focused ion beam—Instrumentation, theory, techniques and pratice, Springer, New York, 2005.
[3] J. Gierak, Semicond. Sci. Technol. 24 (2009) 043001.

[4] J. Gierak, P. Mailly, R. Hawkes, L. Jede, L. Bruchhaus, B. Bardotti, P. Prevel, A. Melinon, R. Perez, J. Hyndman, J.-P. Jamet, A. Ferre, C. Mougin, V. Chappert, P. Mathet, J. Warin, J. Chapman, Appl. Phys. A 80 (2005) 187.
[5] J. Gierak, E. Bourhis, M.N. Merat Combes, Y. Chriqui, I. Sagnes, D. Mailly, P. Hawkes, R. Jede, L. Bruchhaus, L. Bardotti, B. Prevel, A. Hannour, P. Melinon, A. Perez, J. Ferre, J.-P. Jamet, A. Mougin, C. Chappert, V. Mathet, Microelectron. Eng. 78 (2005) 266.
[6] J. Gierak, E. Bourhis, G. Faini, G. Patriarche, A. Madouri, R. Jede, L. Bruchhaus, S. Bauerdick, B. Schiedt, A.L. Biance, L. Auvray, Ultramicroscopy 109 (2009) 457.
[7] A. Bottcher, M. Heil, N. Sturzl, S.S. Jester, S. Malik, F. Perez-Willard, P. Brenner, D. Gerthsen, M.M. Kappes, Nanotechnology 17 (2006) 5889.
[8] F. Ghaleh, R. Köster, H. Hövela, L. Bruchhaus, S. Bauerdick, J. Thiel, R. Jede, J. Appl. Phys. 101 (2007) 044301.
[9] H. Fredriksson, D. Chakarov, B. Kasemo, Carbon 47 (2009) 1335.
[10] S.E. O'Donnell, P. Reinke, J. Vac. Sci. Technol. B 27 (2009) 2209.
[11] P. Melinon, A. Hannour, L. Bardotti, B. Prevel, J. Gierak, E. Bourhis, G. Faini, B. Canut, Nanotechnology 19 (2008) 235305.
[12] M.S. Dresselhaus, R. Kalish, Ion implantation in diamond, graphite and related materials, Springer-Verlag, Berlin, 1992 and references contained therein.
[13] F. Tuinstra, J.L. Koenig, J. Chem. Phys. 53 (1970) 1126.
[14] A.C. Ferrari, J. Robertson, Phys. Rev. B 61 (2000) 14095.
[15] A. Jorio, M.M. Lucchese, F. Stavale, C.A. Achete, Phys. Status Solidi B 246 (2009) 2689.
[16] A.V. Krasheninnikov, K. Nordlund, J. Keinonen, Phys. Rev. B: Condens. Matter 65 (2002) 165423.
[17] F. Tuinstra, J.L. Koenig, J. Chem. Phys. 53 (1970) 1126.
[18] K. Nakamura, M. Kitajima, Phys. Rev. B: Condens. Matter 45 (1992) 78.
[19] L.G. Cançado, K. Takai, T. Enoki, M. Endo, Y.A. Kim, H. Mizusaki, A. Jorio, L.N. Coelho, R. Magalhaes-Paniago, M.A. Pimenta, Appl. Phys. Lett. 88 (2006) 163106.
[20] M.M. Lucchese, F. Stavale, E.H. Martins Ferreira, C. Vilani, M.V.O. Moutinho, R.B. Capaz, C.A. Achete, A. Jorio, Carbon 48 (2010) 1592.
[21] A.V. Krasheninnikov, K. Nordlund, J. Appl. Phys. 107 (2010) 071301.
[22] C.H. Park, L. Yang, Y.W. Son, M.L. Cohen, S.G. Louie, Nat. Phys. 4 (2008) 213.
[23] K. Wakabayashi, Y. Takane, M. Yamamoto, M. Sigrist, N. J. Phys. 11 (2009) 095016.
[24] A.H. Castron Neto, F. Guinea, N.M. Peres, K.S. Novoselov, A.K. Geim, Rev. Mod. Phys. 81 (2009) 109 and references contained therein.
[25] See supplementary materials available for ion implantation on silicon substrate and more information about the geometry of the phenomenological model proposed here.